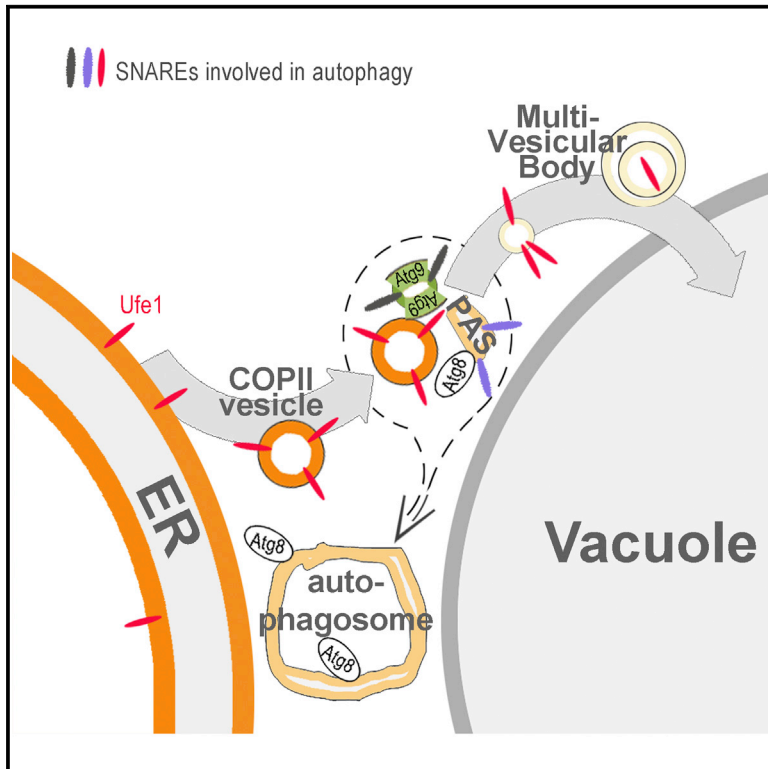# An ER-Localized SNARE Protein Is Exported in Specific COPII Vesicles for Autophagosome Biogenesis

Graphical Abstract

Authors

Leticia Lemus, Juan Luis Ribas, Natalia Sikorska, Veit Goder

Correspondence

vgoder@us.es

In Brief

Lemus et al. show that starvation-induced autophagosome biogenesis in yeast involves the export of endoplasmic reticulum membranes together with the SNARE protein Ufe1 in specific COPII vesicles and their targeting to sites of autophagosome formation.

Highlights

- The ER SNARE protein Ufe1 has a role in autophagosome biogenesis in yeast

- Ufe1 is exported from the ER in specific COPII vesicles upon starvation

- Ufe1 is targeted to cellular structures containing Atg8 and Atg9

- Defective Ufe1 leads to fewer and smaller autophagosomes

CrossMark

CellPress

An ER-Localized SNARE Protein Is Exported in Specific COPII Vesicles for Autophagosome Biogenesis

Leticia Lemus,[1] Juan Luis Ribas,[2] Natalia Sikorska,[1,3] and Veit Goder[1,*]
[1]Department of Genetics, University of Seville, Avenue Reina Mercedes, s/n, 41012 Seville, Spain
[2]Centro de Investigación Tecnología e Innovación de la Universidad de Sevilla, Avenue Reina Mercedes, 41012 Seville, Spain
[3]Present address: Institut de Biologie Moléculaire des Plantes, Centre National de la Recherche Scientifique (CNRS), Université de Strasbourg, 67000 Strasbourg, France
*Correspondence: vgoder@us.es

SUMMARY

The de novo formation of autophagosomes for the targeting of cytosolic material to the vacuole/lysosome is upregulated upon starvation. How autophagosomes acquire membranes remains still unclear. Here, we report that, in yeast, the endoplasmic reticulum (ER)-localized Qa/t-SNARE Ufe1 has a role in autophagy. During starvation, Ufe1 is increasingly exported from the ER and targeted to intracellular sites that contain the autophagy markers Atg8 and Atg9. In addition, Ufe1 interacts with non-ER SNARE proteins implicated in autophagosome formation. Loss of Ufe1 function impairs autophagy and results in fewer and smaller autophagosomes. Unlike conventional cargo, the ER export of Ufe1 is significantly reduced in *sec23-1* cells, which affects the coat protein (COP)II complex, already at the permissive temperature. Under the same conditions, *sec23-1* cells are hypersensitive to starvation and deficient in autophagy. Our data suggest that ER membranes containing Ufe1 are delivered to sites of autophagosome formation in specific COPII vesicles.

INTRODUCTION

Macroautophagy (hereafter autophagy) is a conserved cellular process in response to starvation. A structure called "phagophore" forms in the cytosol at phagophore assembly sites (PAS), elongates while engulfing cytosolic material, and closes to form a double membrane-layered autophagosome that fuses with the vacuole/lysosome for material recycling (Klionsky, 2007; Ohsumi, 2001).

One key question of how autophagosomes are formed concerns the origin of their membranes (Chen and Klionsky, 2011). Growing evidence suggests that several cellular sources can contribute membranes by different and yet poorly understood mechanisms. There is consensus that the endoplasmic reticulum (ER) is a major source for autophagosomal membranes. Transient interconnections between phagophores and ER or specific ER subdomains have been observed both in yeast and mammalian cells and suggest that direct transfer of membranes to growing autophagosomes can occur (Biazik et al., 2015; Graef et al., 2013; Hamasaki et al., 2013; Hayashi-Nishino et al., 2009; Ylä-Anttila et al., 2009). Soluble N-ethylmaleimide-sensitive fusion (NSF) attachment protein receptors (SNARE) proteins with previously described functions in the endocytic and secretory pathways are also involved in autophagosome formation, suggesting that membranes can be equally delivered to autophagosomes through vesicular carriers (Moreau et al., 2011; Nair et al., 2011). Recently, conventional transport vesicles originating from the ER were indirectly (Graef et al., 2013) or directly (Tan et al., 2013) implicated in autophagosome formation in yeast. Together, these data also show that autophagosome formation involves membrane fusion mechanisms that function during conventional membrane traffic under rich growing conditions. During starvation, conventional transport vesicles can be diverted to sites of autophagosome formation by recruiting autophagy-specific modules to tethering complexes (Tan et al., 2013) or by relocalization of fusion activators of the Rab family (Popovic et al., 2012). Whether additional cellular mechanisms specify ER membranes to be used for autophagosome formation during starvation is unclear.

It is known that membrane fusion machineries themselves provide specificity for fusion reactions (McNew et al., 2000). Homo- and heterotypic membrane fusions at the ER are mediated by several distinct and conserved fusion machineries. In yeast, the cycling R/v-SNARE protein Sec22 and the Q/t-SNARE proteins Bet1 and Bos1 are incorporated into budding transport vesicles for fusion with the Golgi apparatus (Newman et al., 1990). The ER-localized Q/t-SNARE proteins Ufe1, Use1, and Sec20 catalyze homotypic ER-ER membrane fusion and heterotypic fusion of retrograde Sec22-containing vesicles with the ER (Anwar et al., 2012; Dilcher et al., 2003; Lewis et al., 1997; Patel et al., 1998). Another ER fusion machinery is Sey1, a dynamin-like GTPase that mediates homotypic ER-ER membrane fusion by an alternative mechanism (Anwar et al., 2012; Hu et al., 2009).

In this study, we addressed the function of specific ER membrane fusion machineries in autophagy in yeast. Our results uncover a cellular mechanism showing that the normally ER-localized SNARE protein Ufe1 is increasingly exported from the ER during starvation. Several independent sets of experiments

CrossMark

lead to a model where ER membranes containing Ufe1 partici-pate in the generation of autophagosomal membranes.

RESULTS

We tested whether Sey1 or Ufe1, which belong to the ER-local-ized fusion machineries, play a role in autophagy. To this end, we used the GFP-Atg8 processing assay in combination with nitrogen starvation. Free GFP is generated as a result of auto-phagy-dependent vacuolar delivery of Atg8, which is an auto-phagosomal marker (Cheong and Klionsky, 2008). Cells with Sey1 deleted did not affect autophagy (Figure 1A). In contrast, cells with the temperature-sensitive *ufe1-1* allele generated free GFP at the permissive (30°C) but not at the non-permissive (37°C) temperature (Figure 1B). The block in autophagy at 37°C was not due to cell death (Figure 1B, lane 12). At the same time, loss of Ufe1 function did not block the autophagy-related constitutive cytoplasm-to-vacuole (Cvt)-pathway (Figure S1A). Although *SEY1* and *UFE1* interact genetically, overexpression of Sey1 could not rescue the autophagy defect in *ufe1-1* cells (Figures S1B and S1C). These data demonstrate that the func-tion of Ufe1 but not of Sey1 is required for starvation-induced autophagy.

To address whether Ufe1 function is required for early or late stages of autophagy, we analyzed cells expressing GFP-Atg8 with live cell fluorescence microscopy. In agreement with the re-sults from western blot analysis, Atg8 was seen inside large spherical structures, the typical pattern of vacuoles, after starv-ing wild-type cells at 30°C or 37°C and *ufe1-1* cells at 30°C (Figure 1C). In *ufe1-1* cells at 37°C, GFP-Atg8 was only seen in punctuate structures after starvation (Figure 1C). Importantly, the number of Atg8 punctuates has multiplied compared to prior of starvation, indicating that autophagosomes or intermediates have formed but that their vacuolar uptake was blocked (Fig-ure 1C). These punctuates were absent in Δ*atg16ufe1-1* cells ruling out autophagy-independent accumulation of Atg8 (Fig-ure 1D). These data suggested that Ufe1 has no essential role in the initiation of autophagosome formation, a fact that was also supported by the finding that lipidation of Atg8 occurred in *ufe1-1* cells at 37°C (Figure S1D).

To analyze the intracellular localizations of Sey1 and Ufe1 before and after starvation, we constructed functional GFP-tagged versions (Figures 2A, S2A, and S2B). Both proteins were initially expressed from their endogenous promoters (EP) and showed weak fluorescence, indicative of low expression levels (Figures 2B and 2C). Under growing conditions, Sey1 was visible in the cortical ER (Figure 2B, "c") and also in the peri-nuclear ER (Figure 2B, "p"), in agreement with previous data (Hu et al., 2009). No change was visible after 5 hr of starvation (Fig-ure 2B). Ufe1 showed a strikingly different behavior. Prior to star-vation, GFP-Ufe1 was visible in the cortical ER (Figure 2C, "c") and also in the perinuclear ER when expressed from the stronger TDH3 promoter (TP-GFP-Ufe1) (Figure S2C). After 5 hr of starva-tion, most of the GFP-Ufe1 was vacuolar (Figures 2C, "v," and S2C). Thus, cellular starvation resulted in ER export and vacuolar targeting of a large fraction of Ufe1. We consistently observed a weak vacuolar signal with both EP-GFP-Ufe1 and TP-GFP-Ufe1 prior to starvation that indicates constitutive ER export of the

protein at a low level under growing conditions (Figures 2C and S2C, "v"). Increased ER export of EP-GFP-Ufe1 also occurred when cells were treated with rapamycin, a drug that induces autophagy independently of starvation (Figure 2D). For a popula-tion-wide and semiquantitative assessment of Ufe1 traffic, we performed western blot analysis. Prior to starvation, a low amount of free GFP was observed in wild-type cells (Figure 2E, lane 1), in agreement with the microscopy data. After 2 hr and 5 hr of starvation, substantial amounts of free GFP had accumu-lated (Figure 2E, lanes 2 and 3). No free GFP was generated in Δ*pep4* cells, which lack vacuolar proteolysis, confirming that Ufe1 was routed to the vacuole upon starvation (Figure 2E, lanes 4–6). No free GFP was generated with EP-Sey1-GFP after up to 5 hr of starvation, in agreement with the microscopy data (Fig-ure 2E, lanes 7–9). To rule out that the increase of Ufe1 export was caused by its tagging, we measured the vacuolar turnover of endogenous Ufe1 in absence and presence of starvation. Endogenous Ufe1 had a low turnover rate under normal growth conditions with only weak stabilization in the Δ*pep4* mutant, implying little or no targeting to the vacuole under these condi-tions, in agreement with previous data (Braun and Jentsch, 2007). Upon starvation, the turn-over of Ufe1 was enhanced and at the same time the protein was now almost fully stabilized in the Δ*pep4* mutant (Figures 2F, "SD-N," and 2G). Thus, endog-enous Ufe1 shows an increase in ER export and targeting to the vacuole upon starvation as well, similar to GFP-Ufe1. It remains to be tested by more rigorous methods if endogenous Ufe1 is constitutively exported from the ER at a low level like GFP-Ufe1.

The increased ER export of Ufe1, but not of Sey1, upon star-vation suggested this to be a selective process rather than bulk ER degradation or ER-phagy that occurs after extended times of starvation or ER stress (Bernales et al., 2007; Hamasaki et al., 2005; Mochida et al., 2015). To support this conclusion, we analyzed tagged versions of two additional and abundant ER membrane proteins, the translocon component Sec63, which is mostly found in ER sheets, and the reticulon protein Rtn1, which is mostly found in ER tubules (Voeltz et al., 2006). In contrast to Ufe1, only minute amounts of vacuolar signal were detected for both proteins after 5 hr of starvation (Figure S2D) and no free GFP was detected after 2 hr of starvation (Fig-ure S2E). Thus, Ufe1 ER export is selective and precedes starva-tion-induced ER-phagy (Mochida et al., 2015). We also tested whether GFP-Ufe1 was a substrate of an autophagy-dependent constitutive ER quality control mechanism (Lipatova and Segev, 2015). This was not the case since free GFP was still increasingly generated from EP-GFP-Ufe1 upon short periods of starvation in autophagy mutants where this pathway is blocked (Figure S2F).

The same result also suggested that Ufe1 was not incorpo-rated into autophagosomes, at least not permanently. However, the starvation-dependent ER export supported a function of Ufe1 in autophagy and furthermore suggested that this function might be outside the ER. We therefore tested if Ufe1 was tar-geted to sites of autophagosome formation by performing co-localization analysis with autophagosome markers using confocal fluorescence microscopy. EP-GFP-Ufe1 and an RFP-tagged version of Atg8 were co-expressed in Δ*ypt7* cells to prevent rapid fusion of autophagosomes with the vacuole (Kiri-sako et al., 1999). Under growing conditions, 0–1 Atg8-labeled
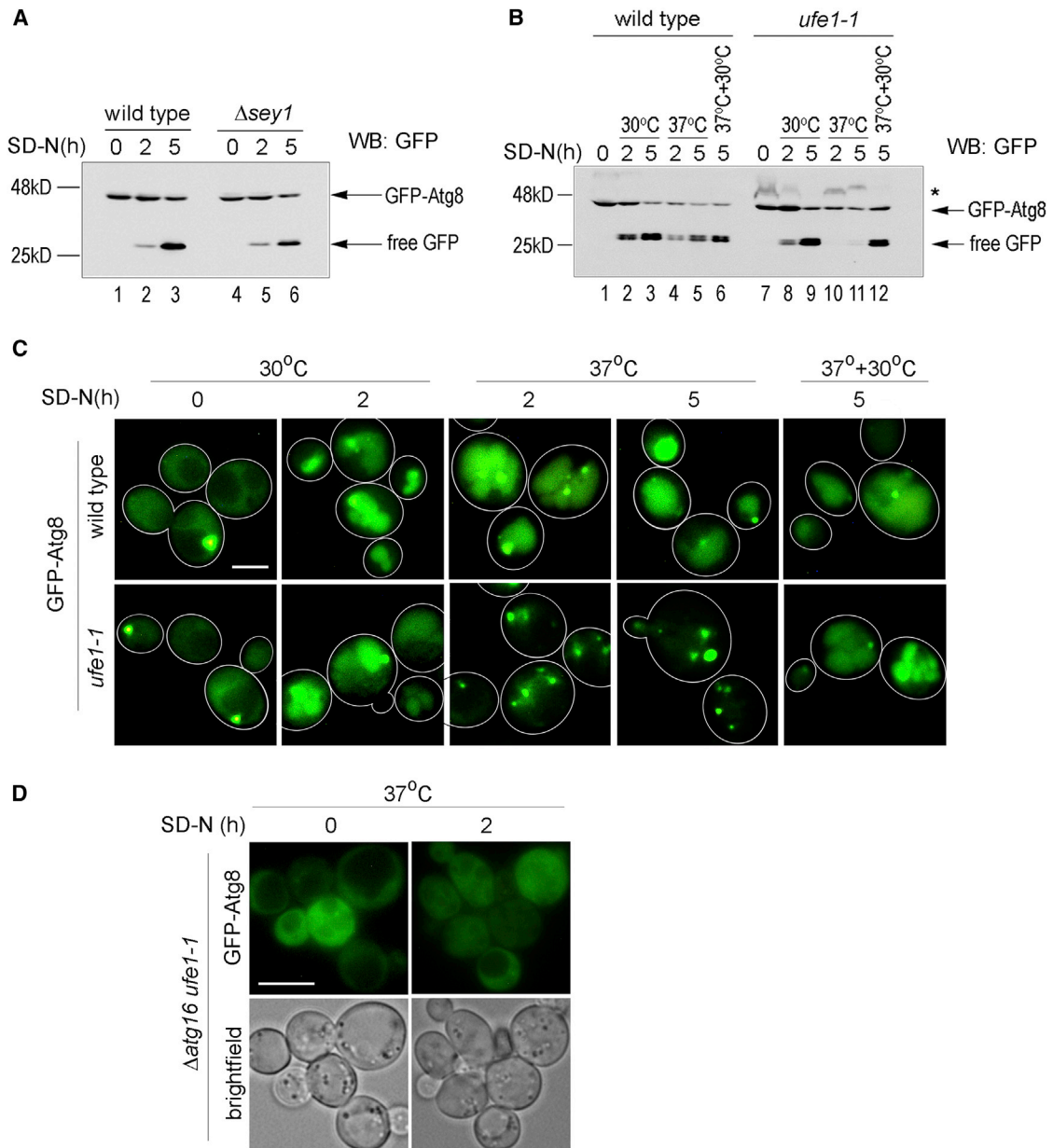
Figure 1. Ufe1 but Not Sey1 Has a Function in Autophagy
(A) GFP-Atg8 processing assay with wild-type cells and Δsey1 cells. Cells were grown to mid-log phase at 30°C and shifted to nitrogen starvation (SD-N) medium for the indicated periods of time. Equal amounts of cell lysates were analyzed by SDS-PAGE and western blotting (WB).
(B) GFP-Atg8 processing assay with wild-type cells and ufe1-1 cells. Like in (A) but, if indicated, shift to 37°C simultaneously with shift to SD-N medium. Lanes 6 and 12: during starvation, cells were incubated for 2 hr at 37°C followed by 3 hr at 30°C. Asterisk indicates unspecific band.
(C) Live cell imaging of wild-type cells and ufe1-1 cells expressing GFP-Atg8. Cells were treated like in (B). Scale bar, 2 μm. Outlines indicate cell borders.
(D) Δatg16ufe1-1 cells expressing GFP-Atg8 were treated like in (B) and imaged before and 2 hr after shifting cells to SD-N medium. Scale bar, 5 μm.
See also Figure S1.

structures per cell were visible in a focal plane indicative of the location of the PAS (Figure 3A, "SD"). Ufe1 appeared in membranes and in additional puncta in Δypt7 cells, the latter of which could represent the fraction of protein that is constitutively exported from the ER but fails to be targeted to the vacuole in this background. More than 60% of Atg8 (PAS) did not show

contact with Ufe1 under these conditions (Figures 3A, "SD," and 3B). At the same time, more than 30% of Atg8-labeled structures were adjacent to Ufe1 (Figure 3B). After 3 hr of starvation, Atg8-labeled structures multiplied, indicative of formation and accumulation of autophagosomes (Figure 3A, "SD-N"). A combined 59% of Atg8 structures were now either adjacent to Ufe1
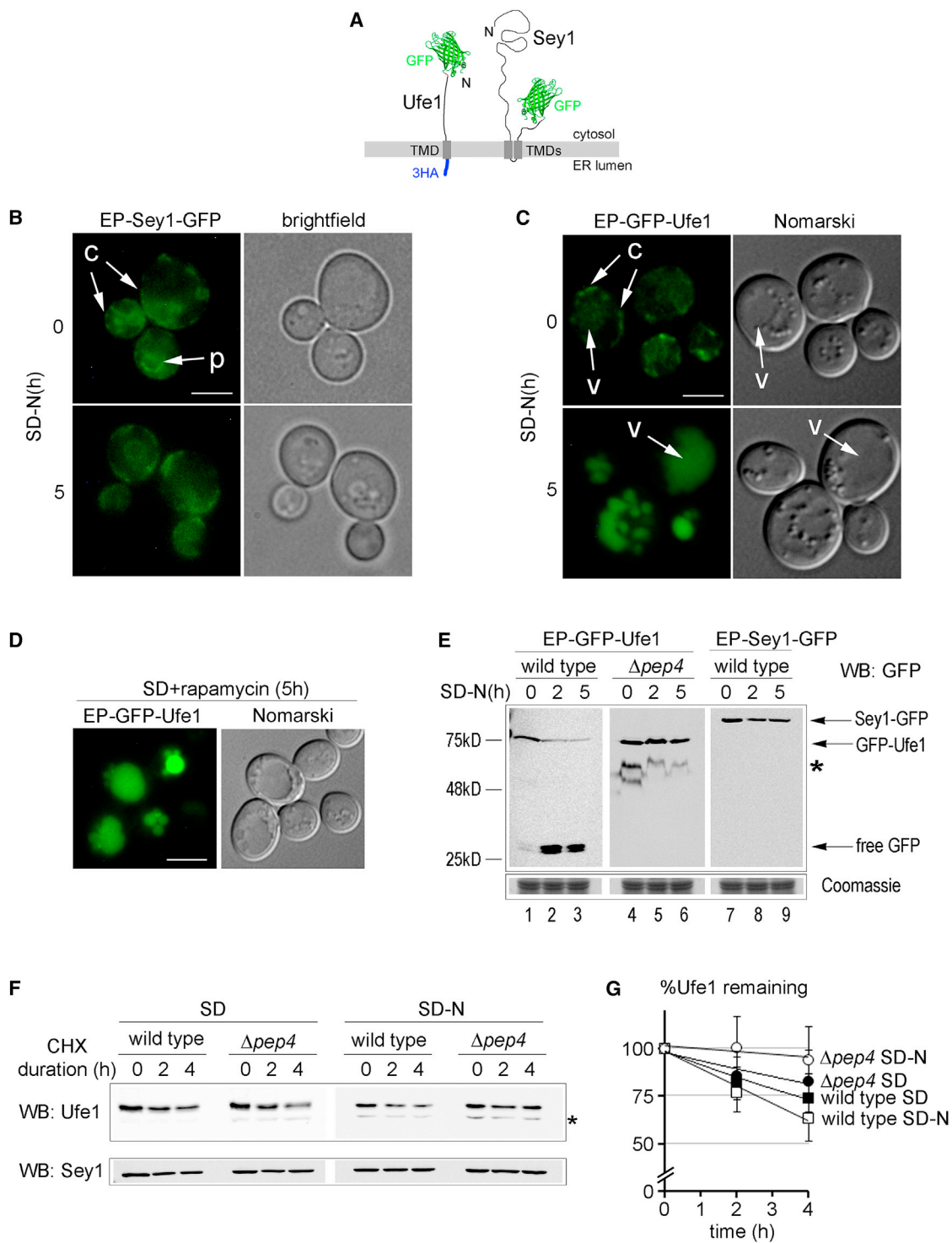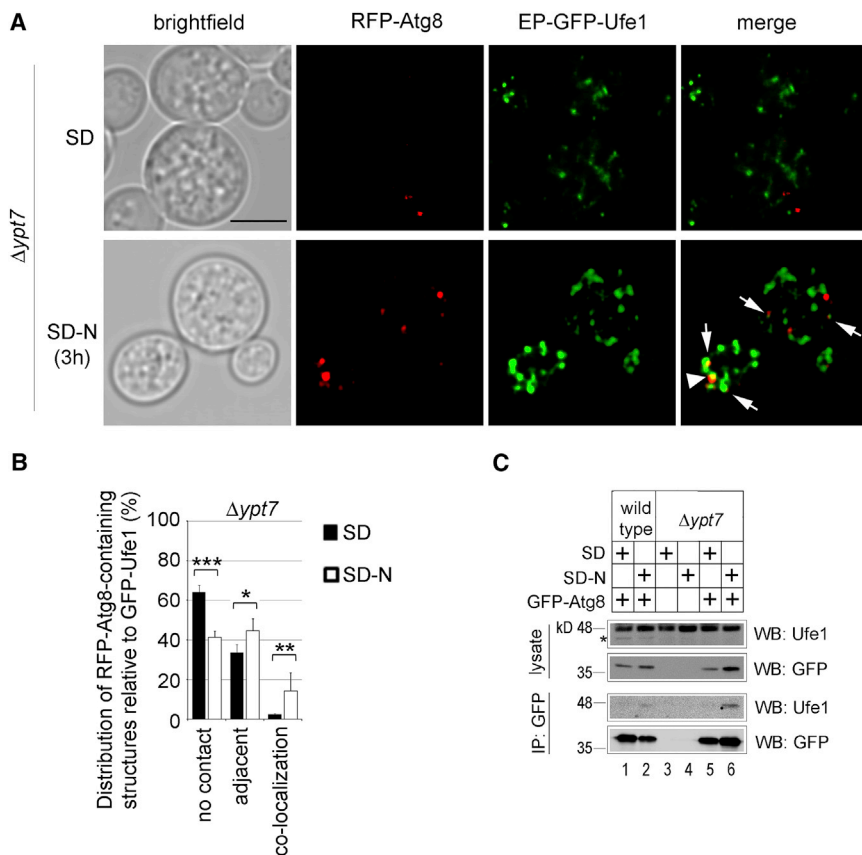
Figure 2. Ufe1 but Not Sey1 Is Increasingly Exported from the ER upon Cellular Starvation

(A) Schematic representation (not to scale) of tagged Ufe1 and Sey1 constructs. GFP was fused to the N terminus of Ufe1 and to the C terminus of Sey1. An additional triple-HA (3HA) tag was fused to the C terminus of Ufe1. TMD, transmembrane domain.

(B and C) Life cell imaging of wild-type cells expressing EP-Sey1-GFP or EP-GFP-Ufe1 before and after starvation at 30°C. c, cortical ER; p, perinuclear ER; v, vacuole. Scale bars, 2 μm.

(D) Life cell imaging of wild-type cells expressing EP-GFP-Ufe1 5 hr after the addition of 200 ng/ml of rapamycin at 30°C. Scale bar, 3 μm.

(legend continued on next page)

A

| brightfield | RFP-Atg8 | EP-GFP-Ufe1 | merge |

Δypt7

SD

SD-N
(3h)

B

Δypt7

Distribution of RFP-Atg8-containing structures relative to GFP-Ufe1 (%)

■ SD
□ SD-N

*** (no contact)
* (adjacent)
** (co-localization)

100 80 60 40 20 0

C

	wild type		Δypt7	
SD	+		+		+
SD-N		+		+	+
GFP-Atg8	+	+		+	+

lysate
kD 48 — * ... WB: Ufe1
35 — ... WB: GFP

IP: GFP
48 — ... WB: Ufe1
35 — ... WB: GFP

1 2 3 4 5 6

Figure 3. Starvation-Dependent Association of Ufe1 with Atg8

(A) Single scan confocal microscopy with Δypt7 cells co-expressing EP-GFP-Ufe1 and RFP-Atg8 before (SD) and after starvation (SD-N) at 30°C. Arrows indicate Ufe1 and Atg8 in adjacent structures. Arrowhead indicates co-localization. Scale bar, 3 μm.

(B) Statistical analysis of the relative distribution from experiments shown in (A). RFP-Atg8 structures prior to starvation (96, n = 140) and after starvation (146, n = 88) were evaluated with respect to contact with GFP-Ufe1. n = number of cells. The mean values and SDs from four individual sets of assessments are shown, see Experimental Procedures. ***$p < 0.001$; **$p < 0.01$; *$p < 0.05$ (unpaired two-tailed Student's t test).

(C) Co-immunoprecipitation (coIP) of endogenous Ufe1 using GFP-Atg8 in combination with chemical crosslinking (see Experimental Procedures). Wild-type cells and Δypt7 cells expressing GFP-Atg8 or control cells were used for coIP experiments before and after starvation followed by SDS-PAGE and western blotting (WB) with the indicated antibodies. Asterisk indicates an unspecific band.

See also Figure S3.

(45%) (Figures 3A, "SD-N," arrows, and 3B) or co-localized (14%) (Figures 3A, "SD-N," arrowhead, and 3B).

Using the same background, co-immunoprecipitation (coIP) experiments with cells co-expressing GFP-Atg8 and TP-Ufe1-3HA showed a starvation-dependent physical interaction between the two proteins (Figure S3). By using coIP in combination with in vivo crosslinking, we also found a starvation-dependent physical interaction between GFP-Atg8 and endogenous (non-tagged) Ufe1 (Figure 3C, lanes 3–6). A faint but reproducible physical interaction was also detectable in wild-type cells (Figure 3C, lanes 1 and 2), suggesting that the interaction is normally transient. Together with the microscopy data, it shows that Ufe1 is targeted in a starvation-dependent manner to cellular sites of autophagosome formation.

An important cytosolic pool of tubo-vesicular membranes for autophagosome formation contains the membrane protein Atg9 and is known to exchange material with the Golgi apparatus and with endosomes (Mari et al., 2010; Ohashi and Munro, 2010; Reggiori et al., 2004; Yamamoto et al., 2012). In yeast, cellular levels of Atg9 correlate with the number of autophagosomes that can be generated, supporting the ascribed role of Atg9 as a membrane carrier (Jin et al., 2014). To test whether Ufe1 comes into contact with Atg9, we performed a co-localization analysis in Δypt7 cells co-expressing EP-GFP-Ufe1 and Atg9mCherry. Atg9 is synthesized at the ER but rapidly exported to the cytoplasmic membrane pool with no ER staining visible at steady state (Figure 4A, "SD") (Mari et al., 2010; Yamamoto et al., 2012). At growing conditions, only 5% of Atg9-containing structures co-localized with Ufe1 (Figures 4A, "SD," arrowhead, and 4B). A significant population of Atg9-containing structures (33%) was adjacent to Ufe1 puncta that are visible in the Δypt7 background under the same conditions (Figures 4A, "SD," arrows, and 4B). After starvation, Atg9-containing structures that co-localized with Ufe1 increased to 32% (Figures 4A, "SD-N," arrowheads, and 4B) and those that were adjacent to Ufe1 to

(E) Wild-type cells and Δpep4 cells expressing EP-GFP-Ufe1 or EP-Sey1-GFP before and after different times of starvation were analyzed by SDS-PAGE and western blotting (WB). The same samples were run on a separate gel and stained with Coomassie to control for general protein content. Asterisk indicates unspecific bands.

(F) Vacuolar turnover of endogenous Ufe1 during normal cell growth (SD) and during starvation (SD-N) was measured using wild-type cells and Δpep4 cells in combination with cycloheximide (CHX) (see Experimental Procedures). Equal aliquots were removed from cell cultures at indicted times and analyzed by SDS-PAGE and western blotting (WB). Same membranes were cut and stained individually with antibodies against Ufe1 or Sey1. Asterisk indicates a non-specific band.

(G) Statistical analysis of remaining intracellular Ufe1 from experiments performed in (F). The mean values and SDs from four individual sets of experiments are shown.

See also Figure S2.

A

	brightfield	Atg9mCherry	EP-GFP-Ufe1	merge
Δypt7 — SD				
Δypt7 — SD-N (3h)				

B

C
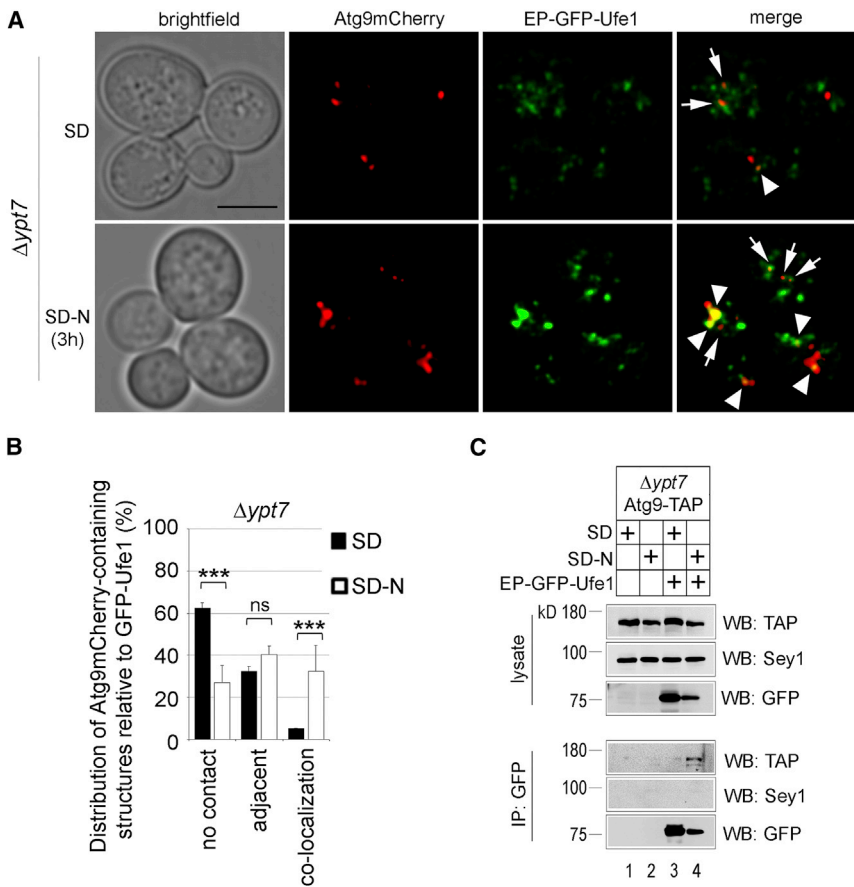
Figure 4. Starvation-Dependent Association of Ufe1 with Atg9

(A) Single scan confocal microscopy with Δypt7 cells co-expressing EP-GFP-Ufe1 and Atg9mCherry before (SD) and after starvation (SD-N) at 30°C. Arrows indicate Ufe1 and Atg9 in adjacent structures. Arrowheads indicate co-localization. Scale bar, 3 μm.

(B) Statistical analysis of the relative distribution from experiments shown in (A). Atg9mCherry structures prior to starvation (243, n = 135) and after starvation (219, n = 65) were evaluated with respect to contact with GFP-Ufe1. n = number of cells. The mean values and SDs from four individual sets of assessments are shown (see Experimental Procedures). ***p < 0.001; not significant (NS) p > 0.05 (unpaired two-tailed Student's t test).

(C) CoIP of Atg9-TAP using EP-GFP-Ufe1. Δypt7 cells co-expressing Atg9-TAP and EP-GFP-Ufe1 or control cells were used for coIP experiments (see Experimental Procedures) before and after starvation followed by SDS-PAGE and western blotting (WB). Same membranes were cut and individually stained with the indicated antibodies. See also Figure S4.

sicular bodies (MVBs), whose fusion with the vacuole also depends on Ypt7. When we expressed EP-GFP-Ufe1 in Δvps4 and Δvps32 cells, which are defective in the generation of MVBs, we did not detect free GFP (Figure S4E). The same result was obtained by fluorescence microcopy showing that vacuolar uptake after cellular starvation depends on MVBs (Figure S4F). This method also revealed that the minor fraction of GFP-Ufe1 that is constitutively exported under growing conditions accumulated in a single spot in Δvps32 cells, typical for a prevacuolar endocytic compartment formed in this mutant, termed the class E compartment (Figure S4F) (Piper et al., 1995). After starvation, Ufe1 was accumulated in multiple puncta per cell (Figure S4F) although the class E compartment is known to remain coalesced in a single spot (Müller et al., 2015). This supports the idea that starvation-dependent export of Ufe1 has a distinct cellular function compared to the constitutively exported minor fraction under growing conditions.

The regulation of autophagosome biogenesis affects autophagosome sizes and their numbers (Jin and Klionsky, 2014). Given the connection of Ufe1 to Atg9 and to general membrane traffic, we addressed whether Ufe1 function affects autophagosome sizes and/or their numbers. To measure sizes of autophagosomes, we performed thin-section electron microscopy. To prevent breakdown of autophagosomes inside the vacuole, cells where treated with the protease inhibitor PMSF during starvation. Larger numbers of autophagosomes inside the vacuole, also called autophagic bodies (ABs), were frequently seen in wild-type cells, as expected (Figure 5A, left panel, arrows). In agreement with fluorescence microscopy data, ufe1-1 cells failed to
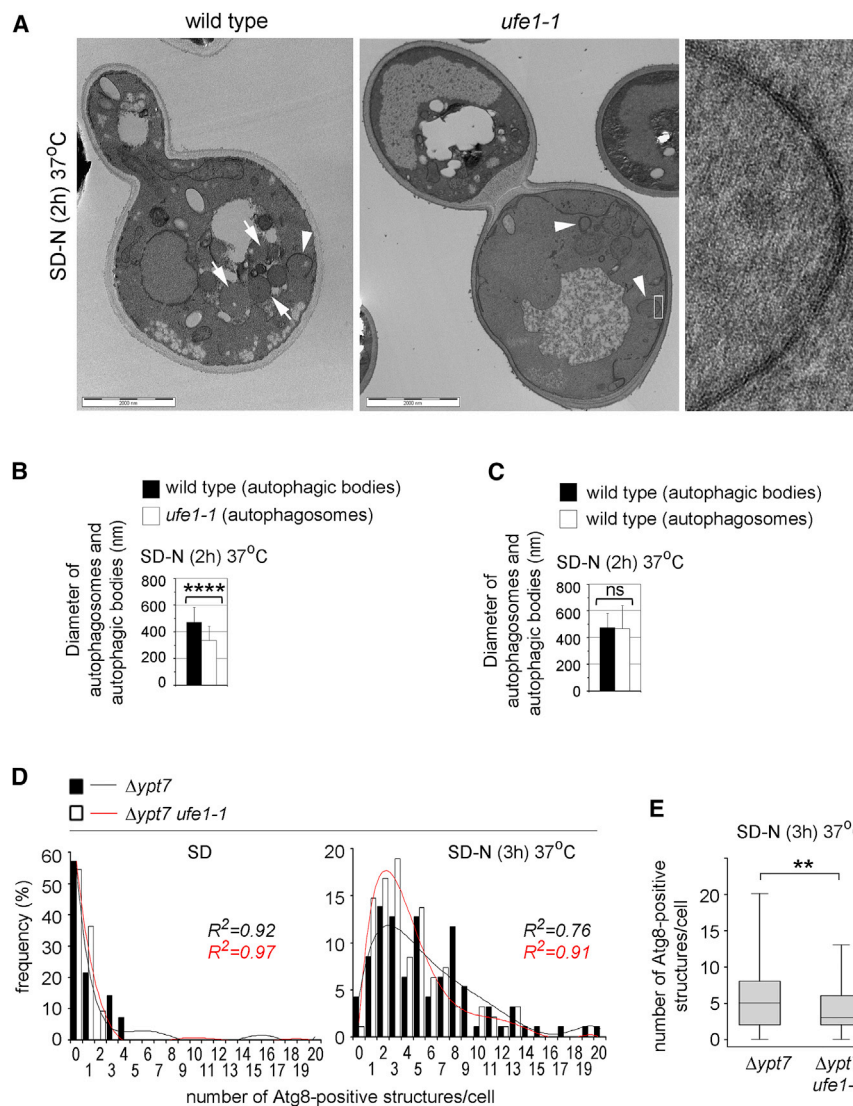
40% (Figures 4A, "SD-N," arrows, and 4B). This shows that during starvation, Ufe1-containing membranes increasingly target to sites that contain Atg9.

To test for a physical interaction, we co-expressed EP-GFP-Ufe1 and a chromosomally TAP-tagged version of Atg9 that was functional (Figure S4A) in Δypt7 cells and performed coIP experiments. We could coIP both proteins in a starvation-dependent manner (Figure 4C, lanes 3 and 4). We did not detect Sey1 among the coIP proteins, showing a high level of specificity (Figures 4C and S4B). Physical interaction was also seen in the reverse pull-down using Atg9-TAP and TP-GFP-Ufe1 (Figure S4C). These data support a direct function for ER membranes containing Ufe1 in autophagosome formation. Although the physical interaction could suggest an exclusive functional link of Ufe1 to Atg9 during starvation, we did see clear differences in the behavior of GFP-Atg8 in Δatg9 cells compared to ufe1-1 cells (Figure S4D, compare to Figure 1C), showing that the function of Ufe1 during autophagy is not linked exclusively to Atg9.

Since the ultimate vacuolar uptake of Ufe1 can occur independent of autophagosome formation (Figure S2F), we addressed the mechanism of Ufe1 transport from sites of autophagosome formation to the vacuole. The observation that Ufe1 accumulated in multiple puncta in Δypt7 cells also after starvation suggested that vacuolar uptake could proceed through multivesicular bodies...

Figure 5. Ufe1 Function Affects Size and Number of Autophagosomes and Their Fusion with the Vacuole

(A) Analysis of wild-type cells and *ufe1-1* cells by electron microscopy after 2 hr of starvation at 37°C in presence of PMSF. Arrows indicate examples of autophagic bodies (ABs) inside the vacuole of a wild-type cell; arrowheads indicate cytosolic autophagosomes in a wild-type cell and in a *ufe1-1* cell. The boxed section of the middle panel is enlarged on the right to illustrate the autophagosomal double membrane. Scale bars, 2,000 nm.

(B) Diameters of ABs (n = 184) in wild-type cells and of autophagosomes (n = 52) in *ufe1-1* cells obtained from (A) were measured with iTEM software. The mean values and SDs are shown. ****p < 0.0001 (unpaired two-tailed Student's t test).

(C) Comparison of the diameters of occasionally visible autophagosomes (n = 15) (arrowhead in A) with ABs in wild-type cells. The mean values and SDs are shown. NS p > 0.05 (unpaired two-tailed Student's t test).

(D) Determination of numbers of Atg8-positive structures. Δ*ypt7* and Δ*ypt7ufe-1* cells expressing GFP-Atg8 were analyzed before and after starvation at 37°C using laser scanning fluorescence microscopy in combination with three-dimensional reconstruction (see Supplemental Experimental Procedures and Figure S5A). Scans from 14 and 94 Δ*ypt7* cells and from 22 and 95 Δ*ypt7ufe-1* cells were analyzed before and after starvation, respectively, at 37°C. The distribution of cells containing a particular number of GFP-Atg8-positive structures is shown in histograms together with polynomial regression lines and their respective R^2 values.

(E) Box plot together with statistical analysis of the results obtained from (D). **p < 0.01 (two-sample F-test for variances).

See also Figure S5.

show ABs but often showed cytosolic autophagosomes, identifiable by a double membrane that enclosed material with the same electron-density like the surrounding cytosol (Figure 5A, middle panel, arrow heads, right panel). The majority of cytosolic autophagosomes in *ufe1-1* cells appeared spherical and closed, revealing no formation defect. Confocal laser scanning microscopy in combination with 3D reconstruction with *ufe1-1* cells expressing GFP-Atg8 also showed hollow structures that were closed in cross section (Figures S5A and S5B). However, the diameters of autophagosomes in *ufe1-1* cells were significantly smaller (335 ± 107 nm) than ABs in wild-type cells (472 ± 112 nm) (Figure 5B). To exclude that ABs differed in size from cytosolic autophagosomes, we measured the occasionally detectable cytosolic autophagosomes in wild-type cells (Figure 5A, left panel, arrow head). Both were indistinguishable in size from one another: 472 ± 112 nm versus 466 ± 174 nm (Figure 5C).

To measure numbers of autophagosomes with used the Δ*ypt7* background, where autophagosomes accumulate in the cytosol.

Δ*ypt7* and Δ*ypt7ufe1-1* cells expressing GFP-Atg8 were analyzed by confocal scanning microscopy in combination with 3D reconstruction before and after starvation for 3 hr at 37°C. The number of Atg8-positive structures per cell multiplied in both strains after starvation but cells with defective Ufe1 contained on average significantly fewer autophagosomes (Figures 5D and E). These data demonstrate that Ufe1 function also affects the number of autophagosomes.

To independently confirm our findings that Ufe1 function affects autophagosome biogenesis, we used a recently developed autophagosome pelleting assay where autophagosomes are accumulated in the Δ*ypt7* background and then pelleted with medium-speed density centrifugation, using GFP-Atg8 as marker (Yamamoto et al., 2012). Control experiments with wild-type cells, Δ*ypt7* cells, and Δ*atg16* cells showed the functionality of the assay (Figure S5C, lanes 1–9). We found that Δ*ypt7ufe1-1* cells showed reduction of more than 50% in pelleting efficiency when compared to Δ*ypt7* cells after starvation at

the non-permissive temperature (Figures S5C, lanes 10–15, and S5D), confirming a defect in autophagosome biogenesis under these conditions.

Together, our data show that cells with non-functional Ufe1 produce several distinct phenotypes with respect to autophagy: autophagosomes are reduced in size and number and they are unable to fuse with the vacuole. As a SNARE protein, Ufe1 might be important for all processes. Since Ufe1 is not permanently incorporated into autophagosomes, the observed defect in fusion with the vacuole could be indirect. In attempt to address in which membrane fusions relevant for autophagy Ufe1 participates, we tested the in vivo binding of the Qa-SNARE Ufe1 to non-ER Qb/c- or R-SNAREs with a role in autophagosome formation or in autophagosome vacuole fusion. The Qb-SNARE Vti1 and the R-SNARE Ykt6 are involved in autophagosome formation (Ishihara et al., 2001; Nair et al., 2011). Both SNARE proteins could be coIP with TP-GFP-Ufe1 after starvation (Figure S5E). In a control experiment, the R-SNARE protein Nyv1 with no role in autophagy (Nair et al., 2011) failed to bind to TP-GFP-Ufe1 (Figure S5E). Likewise, the Qb/c SNARE Vam7, with a well-established role in fusion of autophagosomes with the vacuole did not bind to Ufe1 (Figure S5F). Together, these results support a role for Ufe1 in the biogenesis of autophagosomes, whereas the fusion defect of autophagosomes with vacuoles could be indirect.

Next, we addressed the cellular pathway for the export of Ufe1 from the ER. Export of cargo from the ER mostly depends on the early secretory pathway and is mediated by COPII vesicles (Miller and Schekman, 2013). We expressed EP-GFP-Ufe1 in temperature-sensitive mutants of the early secretory pathway (sec18-1, sec22-3) part of which were COPII mutants (sec13-1, sec23-1, sec31-1) and performed fluorescence microscopy. After starvation, Ufe1 was visible inside the vacuole at the permissive (22°C) and at the non-permissive temperature (37°C) in wild-type cells (Figure 6A). In sec22-3, sec13-1, and sec18-1 cells, vacuolar signal was visible at 22°C but not at 37°C, indicating that the ER exit of Ufe1 relied on the early secretory pathway and on COPII vesicles (Figure 6A). Two mutants produced unusual phenotypes. In sec23-1 cells, ER exit of Ufe1 appeared to be blocked even after starvation at 22°C (Figure 6A). In sec31-1 cells, ER exit of Ufe1 still occurred even at 37°C, and Ufe1 was visible inside the vacuole to an elevated extent also prior to starvation (Figure 6A). Western blot analysis with cell lysates from the same experiments confirmed that sec23-1 cells produced severely reduced amounts of free GFP at 22°C compared to control cells, whereas sec31-1 cells showed elevated levels of free GFP prior to starvation and increasing amounts of free GFP after starvation at 37°C, comparable with wild-type cells, in agreement with the microscopy data (Figures 6B and 6C). In contrast to these phenotypes during starvation, both mutants show normal growth at 22°C, indicating a functional secretory pathway, and no growth at 37°C, indicating a blocked secretory pathway, as expected (Figure S6A). However, it was known previously that the sec31-1 mutant is less restrictive at 37°C during starvation, probably as a result of a compensatory mechanism (Hamasaki et al., 2003). At the same time, it is unknown whether sec23-1 cells possess a similar starvation-dependent difference in sensitivity at 22°C.

To address this issue, we measured the ER export of the model substrate CPY during starvation in sec23-1 and sec31-1 cells. In agreement with published data (Hamasaki et al., 2003), sec31-1 cells showed CPY maturation comparable with that of wild-type cells at 37°C, showing that the observed Ufe1 export is part of a general phenomenon seen with sec31-1 cells (Figures S6B and S6C). On the other hand, CPY maturation was comparable between wild-type cells and sec23-1 cells at 22°C, suggesting that the observed reduction in Ufe1 export under the same conditions is not a general phenomenon (Figures S6B and S6C). To confirm this finding, we tested another substrate. KWW, a chimeric membrane protein, behaved like CPY: its ER export was unaffected at 22°C and reduced at 37°C during starvation (Figures S6D and S6E). Together, these data demonstrate that sec23-1 cells display a specific ER export defect for Ufe1 at the permissive temperature during starvation.

These findings provided us with a tool to test for the correlation of Ufe1 transport with functional autophagy under conditions where the secretory pathway is intact. As expected, the co-localization of GFP-Ufe1 with Atg9mCherry after starvation was strongly reduced in Δypt7sec23-1 cells at 22°C compared to Δypt7 cells (Figure S7A). To test whether sec23-1 cells are deficient for autophagy at 22°C, we plated cells on starvation medium in combination with the vital dye Phloxine B (Tsukada and Ohsumi, 1993). Indeed, of all mutants tested, only sec23-1 cells showed increased sensitivity to starvation over a time course of several days (Figures 7A and 7B). Although autophagy seemed not deficient in sec23-1 cells during shorter periods of starvation when judged visually by transport of GFP-Atg8 to the vacuole with fluorescence microscopy (Figure S7B), it became apparent when we used the GFP-Atg8 processing assay, which yielded fewer free GFP in sec23-1 cells compared to wild-type cells and sec18-1 cells at 22°C (Figures S7C and S7D). These results prompted us to analyze sec23-1 cells at the ultrastructural level. Cells were starved at 22°C in the presence of PMSF and analyzed by electron microscopy. ABs were visible inside the vacuoles of both wild-type cells and sec23-1 cells (Figure 7C). The diameters of ABs that were generated under these conditions and in this background did not differ significantly between wild-type cells (320 ± 61 nm) and sec23-1 cells (345 ± 95 nm) (Figure 7D). However, sec23-1 cells contained on average markedly fewer ABs than wild-type cells (Figure 7E). A statistical analysis for which we included results obtained with sec18-1 cells revealed that the reduction in the number of autophagosomes in sec23-1 cells was significant (Figure 7F). Together, these data reveal that sec23-1 cells are deficient in autophagosome biogenesis at the permissive temperature. This deficiency correlates with the observed specific reduction in export of Ufe1 from the ER and lend independent support to a role of Ufe1-containing ER membranes in the biogenesis of autophagosomes.

DISCUSSION

Our data show that the Qa/t-SNARE Ufe1 plays a role in autophagy. In combination with the observed particular itinerary of Ufe1 during starvation, our findings reveal that autophagy-specific regulation of membrane traffic involves the mobilization of
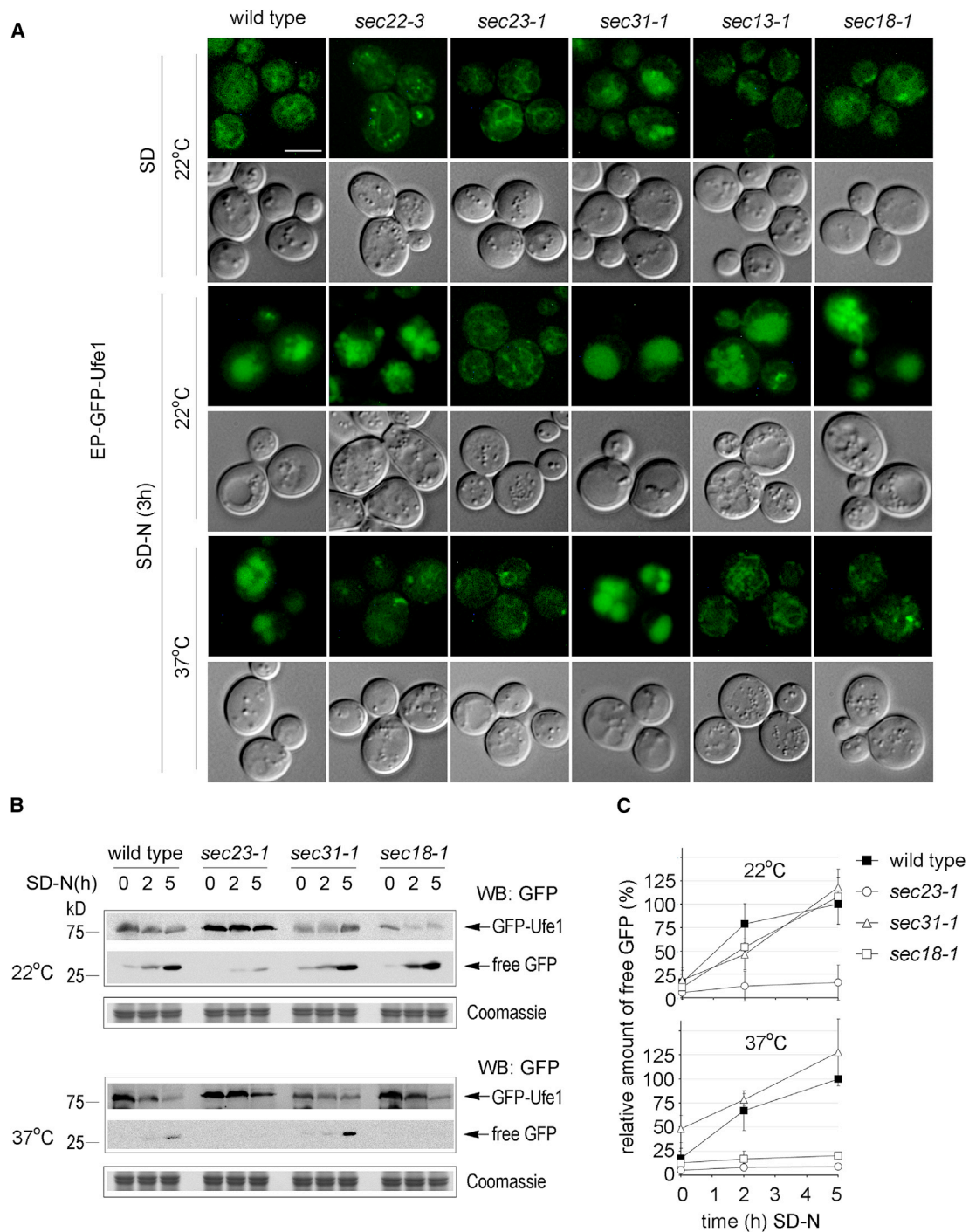
Figure 6. ER Export of Ufe1 Depends on the Secretory Pathway and Is Hypersensitive to the *sec23-1* Mutation

(A) Live cell fluorescence microscopy of wild-type cells and the indicated mutant strains expressing EP-GFP-Ufe1 before and after starvation at the indicated temperatures. Scale bar, 3 μm.

(B) GFP processing assay. The indicated mutants expressing EP-GFP-Ufe1 were starved at the indicated temperatures and analyzed by SDS-PAGE and western blotting (WB). The upper parts of the membranes were overexposed to reveal the fainter GFP-Ufe1 bands. A lower part of the gel was stained with Coomassie as loading control.

(C) Quantifications of free GFP generated in wild-type cells and mutant cells from experiments shown in (B). The amount of free GFP generated in individual strains at different times was normalized to the amount of free GFP generated after 5 hr starvation in wild-type cells (set to 100%) within the same set of experiments. The mean values and SDs from at least three independent sets of experiments are shown.

See also Figure S6.
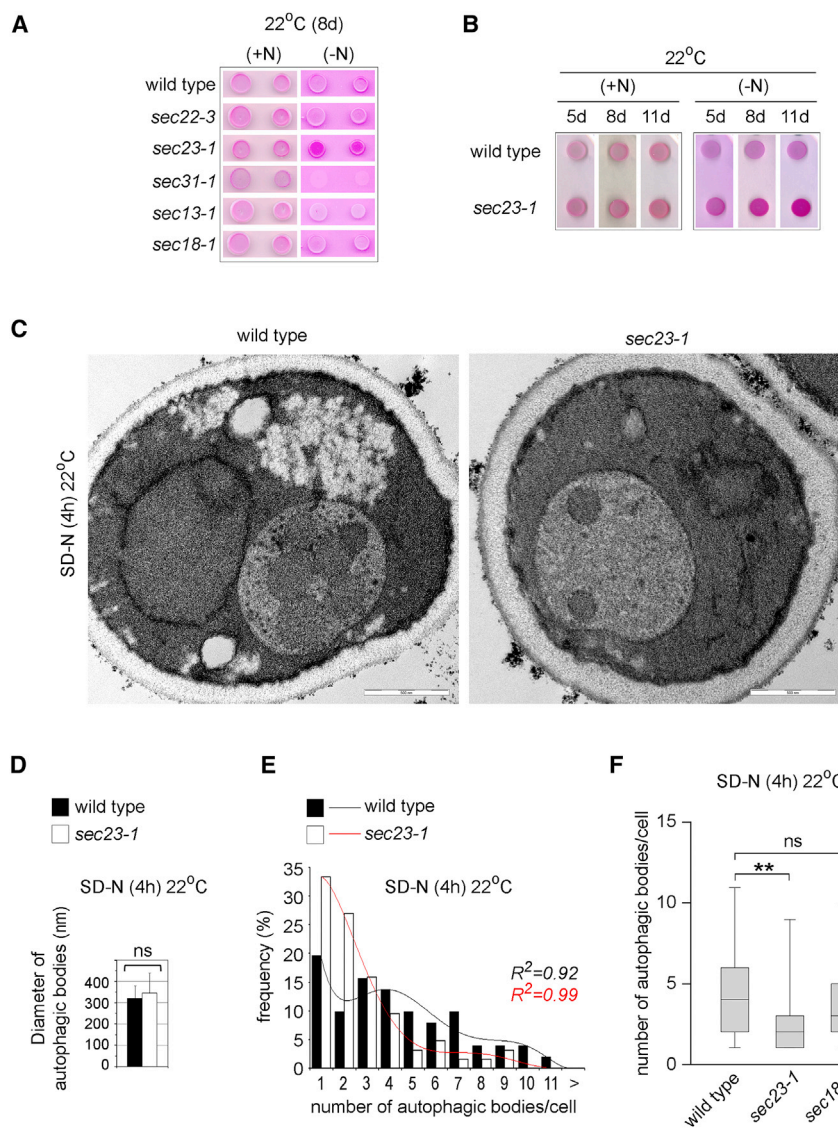
Figure 7. The *sec23-1* Mutant Is Deficient in Autophagy at the Permissive Temperature

(A) Wild-type cells and the indicated mutant cells were spotted in two distinct dilutions onto plates containing minimal medium and the vital dye Phloxine B in presence (+N) or absence (−N) of ammonium sulfate and incubated at 22°C. Plates were imaged after 8 days.

(B) Wild-type cells and *sec23-1* cells were spotted on plates like in (A) and repeatedly imaged after the indicated number of days.

(C) Analysis of wild-type cells and *sec23-1* cells by electron microscopy after 4 hr of starvation at 22°C in presence of PMSF. Representative examples of cells with visible ABs are shown. Scale bars, 500 nm.

(D) The diameters of individual ABs in wild-type cells and in *sec23-1* cells obtained from (C) were measured with iTEM software. The mean values and SDs are shown. NS $p > 0.05$ (unpaired two-tailed Student's t test).

(E) Histogram showing the distribution of cells with a particular number of ABs together with polynomial regression lines and their respective R^2 values. Fifty-one wild-type cells and 63 *sec23-1* cells with at least one AB inside the vacuole from experiments in (C) were imaged and their individual number of ABs counted.

(F). Box plot together with statistical analysis of the results obtained from (E) and including results obtained from the parallel analysis of 37 *sec18-1* cells. NS $p > 0.05$, **$p < 0.01$ (two-sample F test for variances).

See also Figure S7.

(Miller and Schekman, 2013). Interestingly, in mammalian cells, specific (in this case unusually small) COPII vesicles are generated during starvation for the biogenesis of autophagosomes (Ge et al., 2013).

Which membrane fusion steps are catalyzed by Ufe1 during autophagosome biogenesis remains to be elucidated and needs testing in suitable in vitro assays together with candidate partner SNAREs. Our finding that Ufe1 interacts physically with Ykt6 and Vti1 in vivo under conditions of starvation is consistent with the formation of SNARE complexes that do not form under growing conditions but might catalyze particular membrane fusions during starvation, such as for the elongation of phagophores. The common phenotype with respect to autophagosome biogenesis that we have obtained with *ufe1-1* cells at 37°C and with *sec23-1* cells at 22°C was a reduction in the number of autophagosomes. Previous work has established a link between the number of autophagosomes and the available membrane supply for autophagosome biogenesis (Jin et al., 2014). In agreement with these data, inefficient supply of Ufe1-containing membranes in *sec23-1* cells or their inefficient integration into membrane pools for the biogenesis of autophagosomes in *ufe1-1* cells can explain the observed reduction in the number of autophagosomes in

SNARE proteins that are at the core of most membrane fusion machineries and that, in case of Ufe1, are thought to be organelle-specific. This mechanism adds a layer of regulation to the previous findings that starvation leads to a relocalization of membrane fusion regulators of the Rab protein family and to a modulation of membrane tethers in order to direct particular membrane traffic to sites of autophagosome formation (Popovic et al., 2012; Tan et al., 2013).

Our findings suggest that the export of membranes from the ER for the purpose of autophagosome formation depends on specific COPII vesicles. Although we have only limited data, the incorporation of Ufe1 and the particular sensitivity to the *sec23-1* allele for their ER export clearly separate them from "more conventional" transport vesicles. The sensitivity to the *sec23-1* allele, which affects the inner layer of the COPII coat, could reflect specific conformational requirements for coat proteins for the formation of vesicles with different shapes

both cases. The additional phenotype of smaller autophagosomes seen in *ufe1-1* cells at 37°C could reflect a consequence of the SNARE to misfold after having been localized to sites relevant for the biogenesis of autophagosomes.

Whereas several independent results support a role of Ufe1 in autophagosome biogenesis, we do not have results supporting a role of Ufe1 in the fusion of autophagosomes with the vacuole. Although the failure of binding to Vam7 is a negative evidence, we also could not observe Ufe1 on the vacuolar rim as the expected post-fusion localization. It might be that rapid retrieval followed by targeting to MVBs prevented the detection. In mammalian cells, the Qa/t-SNARE protein syntaxin 17 (STX17) was shown to have an exclusive role in mediating the fusion of autophagosomes with the lysosome (Itakura et al., 2012). Although STX17 is not the sequence homolog of Ufe1, a fraction of the protein is likewise found in the ER membrane where it has a role in initiation of autophagosome formation (Hamasaki et al., 2013). However, for fusing autophagosomes with lysosomes, STX17 is recruited directly to autophagosomes from a cytosolic pool (Itakura et al., 2012). It thus remains to be tested whether the known functions of Ufe1 and STX17 during autophagy contain common and evolutionary conserved features.

Rapid retrieval of Ufe1 from autophagosomal membranes could reflect a cellular mechanism to define membrane identity; it would also serve to permit several rounds of fusion. The ultimate targeting of Ufe1 to the vacuole via MVBs might not be surprising considering the close structural and functional connections of autophagosomes with the endosomal system (Biazik et al., 2015; Müller et al., 2015). Endosomes can exchange lipids and probably other material with Atg9 vesicles (Mari et al., 2010; Ohashi and Munro, 2010). Endosomes are also important suppliers of membranes for autophagosome formation in mammalian cells (Puri et al., 2013).

Our findings open a series of questions that are currently being addressed. Foremost, how is Ufe1 incorporated into ER vesicles and how is it regulated? Are the other ER-localized SNAREs similarly exported during autophagy? What else distinguishes the specific COPII vesicles for the autophagosome biogenesis from vesicles transporting cargo along the secretory pathway? Which membrane fusion reactions are catalyzed by Ufe1 during for the formation of autophagosomes, and what are the partner SNARE proteins for these fusions? Answers to these questions will provide a detailed picture of the contribution of the ER to autophagosome formation by vesicular transport.

EXPERIMENTAL PROCEDURES

Construction of Plasmids and Yeast Strains Used in This Study
A description for the construction of plasmids is given in the Supplemental Experimental Procedures. Yeast strains are listed in Table S1.

Electron Microscopy
Cells were grown to optical density (OD) 600 of 0.5, washed, resuspended in starvation (SD-N) medium (1.7% yeast nitrogen base without amino acids and ammonium sulfate, with 2% glucose) containing 1 mM PMSF and incubated for the indicated times at the indicated temperatures. Cultures were harvested by centrifugation, fixed in 1.5% $KMnO_4$ in water for 20 min at 24°C, washed, and stained with 2% uranyl acetate for 1 hr, dehydrated through a graded series of ethanol and propylene oxide, embedded in Epon resin (Ted Pella), and polymerized at 60°C for 2 days. Thin sections were cut with an

ultramicrotome (Leica UC7) using a diamond knife (Diatome 45°) and examined in a Philips CM10 transmission electron microscope operating at 80 kV. Digital images were acquired with a side port 4 Mpx camera (Veleta, Olympus). The size of autophagosomes was analyzed with iTEM software (Olympus).

GFP-Processing Assays
Cells were grown overnight, diluted to OD 0.2, and regrown for 5 hr, washed, resuspended in SD-N medium, and continued. Removed aliquots were lysed by alkaline treatment (Kushnirov, 2000), resuspended in a cell-density normalized volume of loading buffer, followed by SDS-PAGE and western blotting using anti-GFP antibody (Roche), HRP-conjugated anti-mouse secondary antibody (Roche), and ECL (Pierce) as substrate. Images were taken with a LAS-3000 mini imaging system (Fujifilm) and bands were quantified using Multi-Gauge software (Fujifilm).

Fluorescence Microscopy
Cells were grown to OD 600 of 0.2 at the permissive temperature, washed, resuspended in SD-N medium, incubated for the indicated times, and immediately analyzed by live cell imaging using an Olympus BX61 microscope equipped with a 100×/1.4 PlanApo oil-immersion lens and a conventional FITC cube as well as a DIC prism and polarizer for Normarksi imaging. Images were acquired with a DP70 camera and the DPcontroller software (Olympus). Mutants with temperature-sensitive alleles were shifted to the non-permissive temperature simultaneously with the start of starvation.

Confocal Microscopy
Cells were mildly fixed by addition of 2% of paraformaldehyde (PFA) for 30 min, washed, resuspended in PBS, and scanned with a laser-scanning confocal microscope from Zeiss (LSM 7 Duo) equipped with a binary GaAsP (BiG) module using a Plan-Apochromat objective 63×/1,40 Oil DIC. A 488 nm argon laser (GFP) and a 594 nm helium-neon laser were used (RFP and mCherry).

Co-localization Analysis
For statistical analysis of co-localization ZEN software (ZEISS) was used to project images from individual channels. Structures that entirely overlapped were defined as co-localized, partially overlapping or contacting structures were defined as adjacent, otherwise they were defined as no contact. Counting was performed independently by two individuals and repeated twice.

Cycloheximide Shut-Off Experiments
The shut-off was started by addition of 200 μg/ml cycloheximide (CHX) to exponentially growing or starving cells, as indicated. Equal volume aliquots of cell culture were removed at indicated time points and lysed by alkaline treatment (Kushnirov, 2000). Samples were analyzed by SDS-PAGE followed by western blotting with the indicated antibodies.

CoIP
Cell cultures (200 ml) were grown to mid-log phase, washed, and starved, lysed by grinding in liquid nitrogen (1× PBS, 1 mM EDTA, 1 mM PMSF, and protein inhibitor cocktail [Roche]). Lysates were cleared, solubilized by addition of 1% digitonin (Calbiochem) for 30 min, cleared by centrifugation for 20 min at 100,000 × *g* followed by incubation with GFP-trap resin (Chromotek) or with IgG-coupled magnetic beads (Life Technologies). Washing was done in lysis buffer with 0.5% digitonin followed by elution in SDS-loading buffer.

Chemical crosslinking prior to coIP was done according to Müller et al. (2011). Briefly, freshly prepared PFA was added to cells prior to lysis to a final concentration of 1%, incubated for 20 min at 30°C. Cells were moved to ice for 15 min and PFA was quenched by addition of 500 mM glycine. Cells were lysed, membranes solubilized with 1% Triton X-100 (Sigma) for 30 min, and samples were processed like described above. Prior to performing SDS-PAGE, crosslinks were reversed by incubation of samples at 100°C for 30 min.

Phloxine B Plating Assay
Cells were grown in liquid culture in rich medium and spotted onto plates containing 20 μg/ml Phloxine B (Sigma) in synthetic medium with auxotrophic nutrients and nitrogen base with or without ammonium sulfate.

SUPPLEMENTAL INFORMATION

Supplemental Information includes Supplemental Experimental Procedures, seven figures, and one table and can be found with this article online at http://dx.doi.org/10.1016/j.celrep.2016.01.047.

AUTHOR CONTRIBUTIONS

ACKNOWLEDGMENTS

REFERENCES

Anwar, K., Klemm, R.W., Condon, A., Severin, K.N., Zhang, M., Ghirlando, R., Hu, J., Rapoport, T.A., and Prinz, W.A. (2012). The dynamin-like GTPase Sey1p mediates homotypic ER fusion in S. cerevisiae. J. Cell Biol. *197*, 209–217.

Bernales, S., Schuck, S., and Walter, P. (2007). ER-phagy: selective autophagy of the endoplasmic reticulum. Autophagy *3*, 285–287.

Biazik, J., Ylä-Anttila, P., Vihinen, H., Jokitalo, E., and Eskelinen, E.L. (2015). Ultrastructural relationship of the phagophore with surrounding organelles. Autophagy *11*, 439–451.

Braun, S., and Jentsch, S. (2007). SM-protein-controlled ER-associated degradation discriminates between different SNAREs. EMBO Rep. *8*, 1176–1182.

Chen, Y., and Klionsky, D.J. (2011). The regulation of autophagy - unanswered questions. J. Cell Sci. *124*, 161–170.

Cheong, H., and Klionsky, D.J. (2008). Biochemical methods to monitor autophagy-related processes in yeast. Methods Enzymol. *451*, 1–26.

Dilcher, M., Veith, B., Chidambaram, S., Hartmann, E., Schmitt, H.D., and Fischer von Mollard, G. (2003). Use1p is a yeast SNARE protein required for retrograde traffic to the ER. EMBO J. *22*, 3664–3674.

Ge, L., Melville, D., Zhang, M., and Schekman, R. (2013). The ER-Golgi intermediate compartment is a key membrane source for the LC3 lipidation step of autophagosome biogenesis. eLife *2*, e00947.

Graef, M., Friedman, J.R., Graham, C., Babu, M., and Nunnari, J. (2013). ER exit sites are physical and functional core autophagosome biogenesis components. Mol. Biol. Cell *24*, 2918–2931.

Hamasaki, M., Noda, T., and Ohsumi, Y. (2003). The early secretory pathway contributes to autophagy in yeast. Cell Struct. Funct. *28*, 49–54.

Hamasaki, M., Noda, T., Baba, M., and Ohsumi, Y. (2005). Starvation triggers the delivery of the endoplasmic reticulum to the vacuole via autophagy in yeast. Traffic *6*, 56–65.

Hamasaki, M., Furuta, N., Matsuda, A., Nezu, A., Yamamoto, A., Fujita, N., Oomori, H., Noda, T., Haraguchi, T., Hiraoka, Y., et al. (2013). Autophagosomes form at ER-mitochondria contact sites. Nature *495*, 389–393.

Hayashi-Nishino, M., Fujita, N., Noda, T., Yamaguchi, A., Yoshimori, T., and Yamamoto, A. (2009). A subdomain of the endoplasmic reticulum forms a cradle for autophagosome formation. Nat. Cell Biol. *11*, 1433–1437.

Hu, J., Shibata, Y., Zhu, P.P., Voss, C., Rismanchi, N., Prinz, W.A., Rapoport, T.A., and Blackstone, C. (2009). A class of dynamin-like GTPases involved in the generation of the tubular ER network. Cell *138*, 549–561.

Ishihara, N., Hamasaki, M., Yokota, S., Suzuki, K., Kamada, Y., Kihara, A., Yoshimori, T., Noda, T., and Ohsumi, Y. (2001). Autophagosome requires specific early Sec proteins for its formation and NSF/SNARE for vacuolar fusion. Mol. Biol. Cell *12*, 3690–3702.

Itakura, E., Kishi-Itakura, C., and Mizushima, N. (2012). The hairpin-type tail-anchored SNARE syntaxin 17 targets to autophagosomes for fusion with endosomes/lysosomes. Cell *151*, 1256–1269.

Jin, M., and Klionsky, D.J. (2014). Regulation of autophagy: modulation of the size and number of autophagosomes. FEBS Lett. *588*, 2457–2463.

Jin, M., He, D., Backues, S.K., Freeberg, M.A., Liu, X., Kim, J.K., and Klionsky, D.J. (2014). Transcriptional regulation by Pho23 modulates the frequency of autophagosome formation. Curr. Biol. *24*, 1314–1322.

Kirisako, T., Baba, M., Ishihara, N., Miyazawa, K., Ohsumi, M., Yoshimori, T., Noda, T., and Ohsumi, Y. (1999). Formation process of autophagosome is traced with Apg8/Aut7p in yeast. J. Cell Biol. *147*, 435–446.

Klionsky, D.J. (2007). Autophagy: from phenomenology to molecular understanding in less than a decade. Nat. Rev. Mol. Cell Biol. *8*, 931–937.

Kushnirov, V.V. (2000). Rapid and reliable protein extraction from yeast. Yeast *16*, 857–860.

Lewis, M.J., Rayner, J.C., and Pelham, H.R. (1997). A novel SNARE complex implicated in vesicle fusion with the endoplasmic reticulum. EMBO J. *16*, 3017–3024.

Lipatova, Z., and Segev, N. (2015). A role for macro-ER-phagy in ER quality control. PLoS Genet. *11*, e1005390.

Mari, M., Griffith, J., Rieter, E., Krishnappa, L., Klionsky, D.J., and Reggiori, F. (2010). An Atg9-containing compartment that functions in the early steps of autophagosome biogenesis. J. Cell Biol. *190*, 1005–1022.

McNew, J.A., Parlati, F., Fukuda, R., Johnston, R.J., Paz, K., Paumet, F., Söllner, T.H., and Rothman, J.E. (2000). Compartmental specificity of cellular membrane fusion encoded in SNARE proteins. Nature *407*, 153–159.

Miller, E.A., and Schekman, R. (2013). COPII - a flexible vesicle formation system. Curr. Opin. Cell Biol. *25*, 420–427.

Mochida, K., Oikawa, Y., Kimura, Y., Kirisako, H., Hirano, H., Ohsumi, Y., and Nakatogawa, H. (2015). Receptor-mediated selective autophagy degrades the endoplasmic reticulum and the nucleus. Nature *522*, 359–362.

Moreau, K., Ravikumar, B., Renna, M., Puri, C., and Rubinsztein, D.C. (2011). Autophagosome precursor maturation requires homotypic fusion. Cell *146*, 303–317.

Müller, V.S., Jungblut, P.R., Meyer, T.F., and Hunke, S. (2011). Membrane-SPINE: an improved method to identify protein-protein interaction partners of membrane proteins in vivo. Proteomics *11*, 2124–2128.

Müller, M., Schmidt, O., Angelova, M., Faserl, K., Weys, S., Kremser, L., Pfaffenwimmer, T., Dalik, T., Kraft, C., Trajanoski, Z., et al. (2015). The coordinated action of the MVB pathway and autophagy ensures cell survival during starvation. eLife *4*, e07736.

Nair, U., Jotwani, A., Geng, J., Gammoh, N., Richerson, D., Yen, W.L., Griffith, J., Nag, S., Wang, K., Moss, T., et al. (2011). SNARE proteins are required for macroautophagy. Cell *146*, 290–302.

Newman, A.P., Shim, J., and Ferro-Novick, S. (1990). BET1, BOS1, and SEC22 are members of a group of interacting yeast genes required for transport from the endoplasmic reticulum to the Golgi complex. Mol. Cell. Biol. *10*, 3405–3414.

Ohashi, Y., and Munro, S. (2010). Membrane delivery to the yeast autophago-some from the Golgi-endosomal system. Mol. Biol. Cell *21*, 3998–4008.

Ohsumi, Y. (2001). Molecular dissection of autophagy: two ubiquitin-like sys-tems. Nat. Rev. Mol. Cell Biol. *2*, 211–216.

Patel, S.K., Indig, F.E., Olivieri, N., Levine, N.D., and Latterich, M. (1998). Organelle membrane fusion: a novel function for the syntaxin homolog Ufe1p in ER membrane fusion. Cell *92*, 611–620.

Piper, R.C., Cooper, A.A., Yang, H., and Stevens, T.H. (1995). VPS27 controls vacuolar and endocytic traffic through a prevacuolar compartment in Saccha-romyces cerevisiae. J. Cell Biol. *131*, 603–617.

Popovic, D., Akutsu, M., Novak, I., Harper, J.W., Behrends, C., and Dikic, I. (2012). Rab GTPase-activating proteins in autophagy: regulation of endocytic and autophagy pathways by direct binding to human ATG8 modifiers. Mol. Cell. Biol. *32*, 1733–1744.

Puri, C., Renna, M., Bento, C.F., Moreau, K., and Rubinsztein, D.C. (2013). Diverse autophagosome membrane sources coalesce in recycling endo-somes. Cell *154*, 1285–1299.

Reggiori, F., Wang, C.W., Nair, U., Shintani, T., Abeliovich, H., and Klionsky, D.J. (2004). Early stages of the secretory pathway, but not endosomes, are required for Cvt vesicle and autophagosome assembly in Saccharomyces cer-evisiae. Mol. Biol. Cell *15*, 2189–2204.

Tan, D., Cai, Y., Wang, J., Zhang, J., Menon, S., Chou, H.T., Ferro-Novick, S., Reinisch, K.M., and Walz, T. (2013). The EM structure of the TRAPPIII complex leads to the identification of a requirement for COPII vesicles on the macroau-tophagy pathway. Proc. Natl. Acad. Sci. USA *110*, 19432–19437.

Tsukada, M., and Ohsumi, Y. (1993). Isolation and characterization of auto-phagy-defective mutants of Saccharomyces cerevisiae. FEBS Lett. *333*, 169–174.

Voeltz, G.K., Prinz, W.A., Shibata, Y., Rist, J.M., and Rapoport, T.A. (2006). A class of membrane proteins shaping the tubular endoplasmic reticulum. Cell *124*, 573–586.

Yamamoto, H., Kakuta, S., Watanabe, T.M., Kitamura, A., Sekito, T., Kondo-Kakuta, C., Ichikawa, R., Kinjo, M., and Ohsumi, Y. (2012). Atg9 vesicles are an important membrane source during early steps of autophagosome forma-tion. J. Cell Biol. *198*, 219–233.

Ylä-Anttila, P., Vihinen, H., Jokitalo, E., and Eskelinen, E.L. (2009). 3D tomog-raphy reveals connections between the phagophore and endoplasmic reticu-lum. Autophagy *5*, 1180–1185.